Appl. Phys. B 74, 29–33 (2002)
DOI: 10.1007/s003400100729

Applied Physics B
Lasers and Optics

M. WEBER[1,✉]
G. VON BALLY[1]
A. SHUMELYUK[2]
S. ODOULOV[2]

Reflection-type photorefractive gratings in tin hypotiodiphosphate

[1] Laboratory of Biophysics, Institute of Experimental Audiology, University of Münster, Robert-Koch-Str. 45, 48129 Münster, Germany
[2] Institute of Physics, National Academy of Sciences, 46, Science Avenue, 03650 Kiev-39, Ukraine

Received: 26 June 2001/Revised version: 3 September 2001
Published online: 29 November 2001 •

ABSTRACT Reflection photorefractive gratings recorded by nearly counterpropagating light waves in the near infrared are studied in tin hypothiodiphosphate. The ratios are established for certain electrooptic tensor components responsible for reflection grating recording, and the Debye screening length is evaluated. Reflection holograms of binary objects are recorded.

PACS 42.65.Hw; 42.70.Nq

1 Indroduction

Tin hypotiodiphosphate ($Sn_2P_2S_6$, SPS) is known as a promising photorefractive material for recording in the near infrared with a high beam coupling gain and a rather short decay time [1–4]. As distinct from other photorefractive crystals, this one belongs to the low symmetry group m and therefore possesses 10 different nonvanishing electrooptic coefficients [5], including those that can be used for coupling counterpropagating light waves through reflection gratings. Data on electrooptic properties of SPS are not available at present: We found the estimate for only one (most probably the largest) diagonal component, $r_{111} \simeq 70\,\mathrm{pm/V}$ [6]. Our own estimates from experiments on transmission grating recording gave a nearly doubled value, $r_{111} \simeq 130\,\mathrm{pm/V}$ [7]. Unfortunately, this component cannot ensure an efficient readout of the reflection grating in the samples cut along the crystallographic axis. Therefore, the purposes of this paper are (i) to consider the possibility of reflection grating recording by using the other electrooptic coefficients; (ii) to find the ratios of these electrooptic coefficients and other material parameters, profiting from data on hologram recording; and (iii) to compare the sensitivity for reflection grating recording of SPS with the sensitivity of other photorefractive materials. The recording of the reflection holograms with the image bearing signal beam in the near infrared is also reported in this paper.

2 Experimental procedure

The SPS crystals used were grown in the Institute of Solid State Physics and Chemistry, Uhzgorod State University (Ukraine). The sample K3 – $9 \times 4.5 \times 9\,\mathrm{mm}^3$ along the X, Y, and Z axes, respectively – has all faces optically finished. The plane-wave holographic gratings are recorded with the radiation from a single-mode, single-frequency, diode-pumped Nd^{3+}:YAG laser ($\lambda = 1064\,\mathrm{nm}$, 500 mW output power). If nothing else is mentioned we use an unexpanded laser beam.

Figure 1 shows the schematic of the experiment for reflection grating recording. Two identically polarized light beams enter the sample from opposite faces. Every input beam is tilted a few degrees with respect to the relevant entrance face. The tilt angles are slightly different for the two beams, in order to avoid the propagation of the beam reflected from a face in the direction of the transmitted second beam. Half-wave plates in the signal and reference beams allow the polarization of the recording waves to be rotated.

In this geometry we record and read-out the reflection-type photorefractive gratings. In the presence of the strong pump wave the weak signal wave is amplified inside the sample, due to beam coupling in photorefractive media with a $\pi/2$-shifted grating [1]. Figure 2 shows the typical temporal evolution of the signal wave intensity for two-beam coupling during recording and the intensity of the beam diffracted from the recorded grating during read-out. The steady-state gain is reduced in this sample because of the formation of a supplementary out-of-phase space-charge grating, which is clearly visible in Fig. 2a. This type of grating formation is explained by the presence of the thermally excited carrier mo-

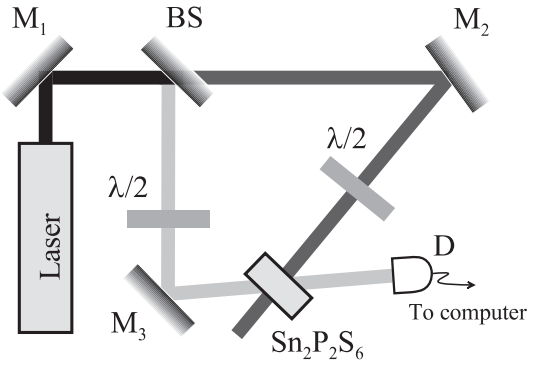

FIGURE 1 Schematic of experimental set-up. BS: beam-splitter; D: detector; M_1, M_2, and M_3: mirrors; $\lambda/2$ half-wave phase retarders. The angles of incidence of the recording waves are out of scale in order to show that the waves are not exactly counterpropagating

✉ Fax: +49-251/83-58536, E-mail: maweber@uni-muenster.de

tion [1]. If the signal wave is blocked after both gratings are recorded until saturation, the intensity of the diffracted wave behaves as shown in Fig. 2b: it drops down to zero within several milliseconds, rises again to a certain value and then decays much more slowly. This behaviour is typical for materials with simultaneous decay of two out-of-phase gratings that possess considerably different time constants [1].

If the recording is stopped when the fast grating is already built-up but the slow out-of-phase grating is not developed, the usual smooth decay is observed with the short decay time. Figure 2c,d show the relevant dynamics of the signal wave intensity during recording and diffracted wave intensity during read-out.

Qualitatively the recording and erasure dynamics for a reflection hologram resembles that known for transmission gratings [1], but the characteristic times for build-up and decay in reflection geometry are somewhat longer, caused by the specific dependence of grating lifetime on spatial frequency [1, 8]. The details of the described dynamics are important for the optimized choice of the exposure and read-out sequence in reflection hologram recording (see Sect. 5).

To characterize reflection gratings the standard exponential gain factor Γ,

$$\Gamma = \frac{1}{\ell} \ln \frac{I_s}{I_s(0)} , \tag{1}$$

has been calculated, where I_s and $I_s(0)$ are the measured intensities of the transmitted signal wave in the presence of the pump beam and without the pump beam, respectively, and ℓ is the sample thickness. The transient peak intensity of the amplified signal wave is taken for the evaluation of the maximum value of Γ.

Figure 3a,b show the polarization dependences of the gain factor for the grating vector $\boldsymbol{K}$ aligned along the OX axis and along the OZ axis, respectively. The polarization angle φ is measured from the OZ direction for Fig. 3a and from the OX direction for Fig. 3b. The total light intensity in this experiment is 40 W/cm^2, and the beam intensity ratio is kept equal to 1:100. A maximum gain factor up to 0.8 cm^{-1} has been achieved for $\boldsymbol{K} || OZ$. For the 9-mm-thick sample the measured diffraction efficiency $\eta = I_{\text{diff}}/(I_{\text{trans}} + I_{\text{diff}})$ of the grating was about 0.01.

For the grating vector aligned along the third direction, orthogonal to the first two, the largest measured gain factor was below ± 0.05 cm^{-1}.

3 Electrooptic properties

The polarization dependences shown in Fig. 3 allow us to evaluate the ratios of the electrooptic coefficients which are involved in the grating recording [8–10]. The expressions describing these polarization dependence can be derived from the general definition of the gain factor for anisotropic photorefractive material with nonlocal nonlinear response [8, 9]:

$$\Gamma = \left[\frac{2\pi\xi(\boldsymbol{e}_R \Delta\varepsilon \boldsymbol{e}_S)}{n\lambda\cos\theta}\right]\left[\frac{1}{1+(2n\ell_s/\lambda)^2}\right] , \tag{2}$$

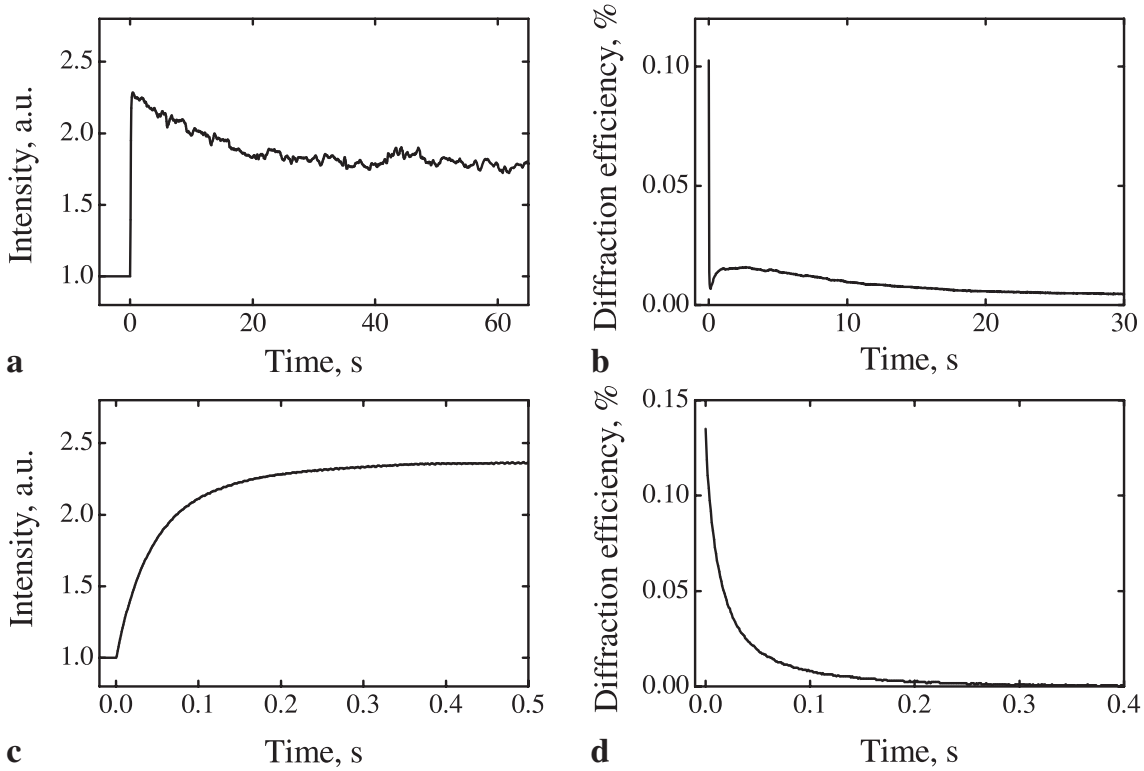

FIGURE 2 Temporal variation of the signal wave intensity during grating recording (**a**, **c**) and diffraction efficiency of the grating during read-out (optical erasure) (**b**, **d**). For **a**, **c** the pump wave is switched on at $t = 0$ s. The signal wave is switched off after 65 s recording time for (**b**) and after 0.5 s recording time for (**d**)

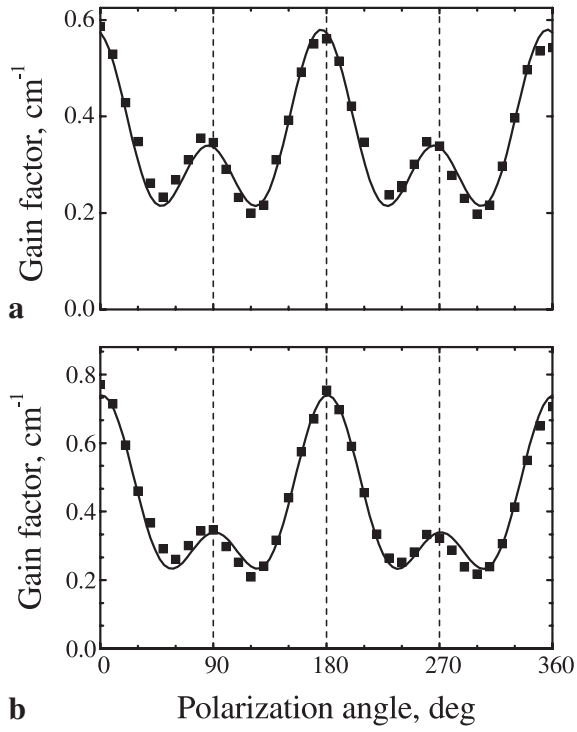

FIGURE 3 Polarization dependences of the gain factory for a reflection grating with the grating vector parallel to **a** the OX axis and **b** the OZ axis. $I_p/I_s \simeq 120$, $I_p = 40\ \mathrm{W/cm^2}$. The *solid lines* represent the best fit of the theoretical dependences [(5) and (6)] for **a** and **b**, respectively

where $\boldsymbol{e}_R$ and $\boldsymbol{e}_S$ are the unit polarization vectors for the two recording waves, n is the unperturbed refractive index (we neglect, for the sake of simplicity, the difference between the refractive indices in three eigenwaves of this optically biaxial crystal), λ is the wavelength, θ is the half-angle between two beams inside the crystal, and ℓ_s is the Debye screening length,

$$\ell_s = 2\pi\sqrt{\frac{\varepsilon\varepsilon_0 k_B T}{e^2 N_{\mathrm{eff}}}}\,, \tag{3}$$

with $\varepsilon\varepsilon_0$ being the dielectric constant, N_{eff} the effective trap density, e the electron charge, k_B the Boltzmann constant, and T the ambient temperature. The factor $\xi < 1$ takes into account imperfect poling of the sample (the presence of a certain amount of 180° domains); it accounts also for the intensity dependence of unknown origin [1]. The dielectric constant is modulated by the space charge field E^{sc} via the Pockels effect. The following expression holds for the particular tensor components $\Delta\varepsilon_{jk}$ [6]:

$$\Delta\varepsilon_{jk} = -\sum_{n=1}^{3}\sum_{m=1}^{3}\sum_{l=1}^{3}\varepsilon_{jn}r_{nml}E_l^{sc}\varepsilon_{mk}\,. \tag{4}$$

For the considered experimental dependences the relevant expressions become

$$\Gamma^x = -\left(\frac{2\pi n^3 E^{sc}\xi^x}{m\lambda\cos\theta}\right)\left[\frac{1}{1+(2n\ell_s^x/\lambda)^2}\right] \times\left(r_{221}\sin^4\varphi + r_{331}\cos^4\varphi\right), \tag{5}$$

$$\Gamma^z = -\left(\frac{2\pi n^3 E^{sc}\xi^z}{m\lambda\cos\theta}\right)\left[\frac{1}{1+(2n\ell_s^z/\lambda)^2}\right] \times\left(r_{223}\sin^4\varphi + r_{113}\cos^4\varphi\right). \tag{6}$$

The subscripts x, z for gain factor, Debye screening length and correction factor ξ indicate that these quantities are taken for the space charge field along the crystallographic axes OX and OZ, respectively (ξ may be anisotropic because of the particular shape of domains with antiparallel spontaneous polarization, e.g. needle-like domains with preferable orientation along certain crystallographic axis or along spontaneous polarization).

The solid lines in Fig. 3a,b are the best fits of the theoretical dependence [(5) and (6)] to the experimental data. A good qualitative agreement of calculated and measured data is evident. From this calculation the ratio of the relevant electrooptic coefficients can be extracted:

$$r_{221}/r_{331} \simeq 0.59\,, \tag{7}$$

$$r_{223}/r_{113} \simeq 0.45\,. \tag{8}$$

Note that the anisotropy of ℓ_s and ξ does not prevent evaluation of these two ratios but makes it impossible to compare, for example, r_{221} with r_{223} in a similar way.

For the third possible orientation of the grating vector $\boldsymbol{K}||OY$ the two-beam coupling gain should be identical to zero, because the relevant components of the Pockels tensor are vanishing ($r_{112} = r_{332} = 0$) [5]. The detected weak coupling originates, most probably, from the imperfect orientation of sample faces to the crystallographic OY orientation.

4 Estimation of the gain factor for reflection geometry

As one can see from (2) and (3) the limiting factors for the gain in photorefractive crystals are related to the finite Debye screening length, which can be comparable or even larger than the grating spacing of the reflection holograms ($\Lambda_R = \lambda/2n$) and the correction factor $\xi < 1$. The Debye screening length can be evaluated from the spatial frequency dependence of the gain factor in transmission geometry. With ℓ_s found in such a way, the ultimate value of the gain factor for the reflection geometry can then be estimated (providing $\ell_s \ll \lambda/2n$) and also the products ξr_{ijk} can be determined.

With this in mind we measure the dependence of the gain factor on fringe spacing Λ by changing the angle between the recording waves in the transmission geometry with $\boldsymbol{K}||OX$. It has been pointed out already [11, 12] that simultaneous consideration of the data for transmission and reflection geometry provides more reliable results on the Debye screening length.

Two beams enter the sample in a plane parallel to the crystal OX axis and both are polarized normal to the plane of incidence. Figure 4 shows the measured data (dots) and the fit with the theoretical dependence [13] given by

$$\Gamma = \left(\frac{4\pi^2\xi r_{221}n^3}{\lambda\Lambda}\right)\left(\frac{k_B T}{e}\right)\left[\frac{1}{1+(\ell_s/\Lambda)^2}\right]. \tag{9}$$

The solid dot represents the measured gain factor in reflection geometry, with the same intensity of the recording

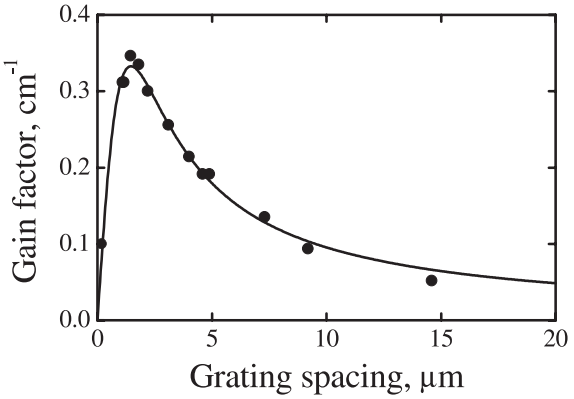

FIGURE 4 Spatial frequency dependence of the gain factor for a transmission grating with the grating vector parallel to the OX axis and light polarized along the OY axis (*open dots*). The *solid dot* marks the measurement for reflection geometry. $I_p/I_s \simeq 100$, $I_p = 3\,\mathrm{W/cm^2}$. The *solid line* shows the best fit of (9) to the experimental data

beams. To ensure the best possible beam overlap when measuring the grating spacing dependence (Fig. 4), we use expanded beams. Therefore, the light intensity and the maximum gain factor are reduced, as compared to the data in Fig. 3a.

All data, for transmission geometry as well as for reflection geometry, are satisfactorily fitted by the same dependence according to (9). From the fit we extract the Debye screening length to be $\ell_s^x \simeq 1.5\,\mu\mathrm{m}$. With the dielectric constant $\varepsilon = 230$, the effective trap density is evaluated, $N_{\mathrm{eff}} \simeq 6.1 \times 10^{15}\,\mathrm{cm^{-3}}$.

From the same fit we find $\xi r_{221} = 6.7\,\mathrm{pm/V}$ and can estimate the ultimate value of the gain factor in reflection geometry, $\Gamma_{\mathrm{ult}}^x \simeq 7.4\,\mathrm{cm^{-1}}$, that might be reached in this crystal with near infrared light, providing the Debye screening length is small enough, $\ell_s \ll \lambda/2n$. It should be remembered that the gain factor for two-beam coupling in SPS is intensity dependent, and Γ_{ult}^x may be even larger for higher intensities of the recording beams. These estimates show that the performance of SPS as a medium for reflection hologram recording still can be largely improved by technological means (by increasing the effective trap density).

An important characteristic of any recording medium is its holographic sensitivity. There is no unified approach in the definition of this parameter [8, 14]. We will use the one that defines holographic sensitivity S_h as

$$S_h = \sqrt{\eta}/WV\,, \tag{10}$$

where η is the diffraction efficiency, V is the fringe visibility, and W is the total energy density at the crystal that is necessary to achieve a given value of η. This is a standard definition of recording material sensitivity in traditional holography [15]. The reciprocal value S_h^{-1} thus describes the intensity necessary to record a grating normalized to $\eta = 1\%$ and $V = 1$. With the total intensity of the recording beams in the sample $I_0 \simeq 20\,\mathrm{W/cm^2}$, a fringe visibility of about 0.08, and an exposure time of 5 ms to reach 0.01 diffraction efficiency, we obtain $S_h^{-1} \simeq 0.08\,\mathrm{J/cm^2}$. This value is comparable to the data for other wide bandgap photorefractive crystals which are used however exclusively with visible light [13].

5 Image recording and reconstruction

It has been mentioned already that tin hypothiodiphosphate ensures the fastest grating recording (in the millisecond range) as compared to any other known wide bandgap ferroelectrics and it features the recording of two out-of-phase photorefractive gratings with charge carriers of different signs [1, 2]. These properties impose some special requirements for holographic image recording and read-out.

Referring to the data presented in Fig. 2 we use two techniques with different time sequences for hologram recording. In the first technique the hologram is recorded until saturation of both gratings (recording time ≥ 200 s) and the diffracted images are piked-up by a CCD camera with a delay of a few seconds. Thus the image is reconstructed near the maximum of the diffraction efficiency (Fig. 2b), and the diffraction from the slow grating is utilized. In this technique the obtained diffraction efficiency is smaller than the maximum value which is due to the fast grating only, but the time constant is much longer and thus the time delay of the readout is less critical.

The alternative technique is based on the recording and reconstruction of only one – the fast – grating. The exposure time is chosen within the interval 0.2–0.5 s and the readout should follow immediately after the signal wave is stopped (see Fig. 2c,d).

To ensure the largest possible refractive index modulation, the grating vector of the holograms is chosen $\boldsymbol{K} \| OZ$ and polarization of the recording beams $\boldsymbol{e}_R$, $\boldsymbol{e}_S$ is oriented nearly parallel to OX. Thus the electrooptic constant r_{113} is used. To profit from the intensity dependence of the gain factor, the intensity of the reference wave in these experiments is up to $60\,\mathrm{W/cm^2}$, while the intensity of the signal (image) wave is $\simeq 0.1\,\mathrm{W/cm^2}$.

Both techniques have been tested with the reconstructed image continuously monitored with an infrared sensitive CCD camera. This allows the brightest diffracted images to be selected from a sequence taken with 200 ms time intervals.

Figures 5–7 represent the images stored and reconstructed from the reflection-type holograms in SPS. In all these figures, panel a shows the image in the signal beam transmitted

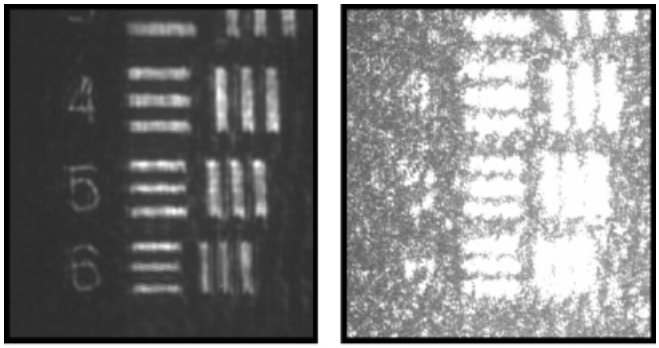

FIGURE 5 Image of the resolution chart transmitted through the sample (**a**) and reconstructed from the reflection hologram (**b**); first type of recording sequence (see text)

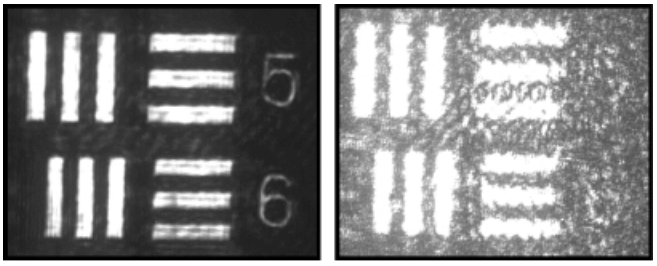

FIGURE 6 Image of the resolution chart transmitted through the sample (**a**) and reconstructed from the reflection hologram (**b**); second type of recording sequence (see text)

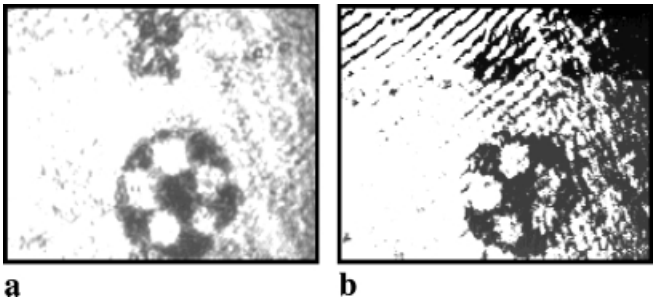

FIGURE 7 Image of a soccer ball transmitted through the sample (**a**) and reconstructed from the reflection hologram (**b**); second type of the recording sequence (see text)

through the sample, while panel b represents the image reconstructed from the hologram. The resolution chart served as an image transparency in Figs. 5 and 6, and a picture of soccer ball was used for Fig. 7.

It should be noted that the image quality and the resolution are limited in this experiment by the optical quality of the sample and, especially, by imperfect polishing of the input–output sample faces. Further development of the growth technology and technology of optical finishing will ensure better spatial resolution typical for reflection-type image holograms.

6 Conclusions

Our experiments prove the possibility of efficient recording of reflection-type photorefractive gratings and reflection holograms in SPS with 1.06 μm radiation of a standard cw Nd^{3+}:YAG laser. A gain factor of about 1 cm^{-1} and a diffraction efficiency of about 0.05 in a 0.9-cm-thick sample are achieved. These parameters can be improved at least for one order of magnitude in samples with an effective trap density high enough to ensure $\ell_s \ll \lambda/2n$.

ACKNOWLEDGEMENTS Financial support of the Deutsche Forschungsgemeinschaft (SFB225) and Alexander von Humboldt Foundation is gratefully acknowledged. We are grateful to A. Grabar and I. Stoyka for the SPS samples.

REFERENCES

1 S. Odoulov, A. Shumelyuk, U. Hellwig, R. Rupp, A. Grabar, I. Stoyka: J. Opt. Soc. Am. B **13**, 2352 (1996)
2 A. Shumelyuk, S. Odoulov, G. Brost: Appl. Phys. B **68**, 959 (1999)
3 M. Weber, F. Rickermann, G. von Bally, A. Shumelyuk, S. Odoulov: Optik **111**, 333 (2000)
4 J. Seres, S. Stepanov, S. Mansurova, A. Grabar: J. Opt. Soc. Am. B **17**, 1986 (2000)
5 J. Nye: *Physical Properties of Crystals* (Oxford University Press, Oxford 1972)
6 R.O. Vlokh, Yu.M. Vysochanski, A.A. Grabar, A.V. Kityk, V.Yu. Slivka: Inorg. Mater. **27**, 570 (1991)
7 A. Shumelyuk, S. Odoulov, D. Kip, E. Krätzig: Appl. Phys. B **72**, 707 (2001)
8 M.P. Petrov, S.I. Stepanov, A.V. Khomenko: *Photorefractive Crystals in Coherent Optical Systems* (Springer, Berlin, Heidelberg 1991)
9 K. Shcherbin, S. Odoulov, R. Litvinov, E. Shandarov, S. Shandarov: J. Opt. Soc. Am. B **13**, 2268 (1996)
10 U.B. Dorfler, R. Piechatzek, Th. Woike, M.K. Imlau, V. Virth, L. Bohaty, T. Volk, R. Pankrath, M. Woehleke: Appl. Phys. B **68**, 843 (1999)
11 K. Shcherbin, A. Shumelyuk, S. Odoulov, P. Fochouk, G. Brost: SPIE Proc. **2795**, 236 (1996)
12 Ph. Delaye, L.A. de Montmorillon, I. Biaggo, J.C. Launay, G. Roosen: Opt. Commun. **134**, 580 (1997)
13 N. Kukhtarev, V. Markov, S. Odoulov, M. Soskin, V. Vinetskii: Ferroelectrics **22**, 949 (1979)
14 S.I. Stepanov: Rep. Prog. Phys. **57**, 39 (1994)
15 R.J. Collier, C.B. Burckhardt, L.H. Lin: *Optical Holography* (Academic, London 1971)